Evol Ecol (2008) 22:771–799
DOI 10.1007/s10682-007-9209-1

ORIGINAL PAPER

Joint evolution of predator body size and prey-size preference

Tineke A. Troost · Bob W. Kooi · Ulf Dieckmann

Received: 3 June 2005 / Accepted: 3 September 2007 / Published online: 9 November 2007
© Springer Science+Business Media B.V. 2007

Abstract We studied the joint evolution of predator body size and prey-size preference based on dynamic energy budget theory. The predators' demography and their functional response are based on general eco-physiological principles involving the size of both predator and prey. While our model can account for qualitatively different predator types by adjusting parameter values, we mainly focused on 'true' predators that kill their prey. The resulting model explains various empirical observations, such as the triangular distribution of predator–prey size combinations, the island rule, and the difference in predator–prey size ratios between filter feeders and raptorial feeders. The model also reveals key factors for the evolution of predator–prey size ratios. Capture mechanisms turned out to have a large effect on this ratio, while prey-size availability and competition for resources only help explain variation in predator size, not variation in predator–prey size ratio. Predation among predators is identified as an important factor for deviations from the optimal predator–prey size ratio.

Keywords Body size · Prey-size preference · Size-dependency · Upper triangularity

Introduction

The range of body sizes encountered in nature is enormous. A bacterium with full physiological machinery has a volume of 0.25×10^{-18} m^3, while a blue whale has a volume of up to 135 m^3. These body sizes are associated with the different scales in time and space in which organisms live, and reflect the differences in physiological processes and life histories. A wide range is also found in the prey-size preference of predators: consider, for

T. A. Troost (✉) · B. W. Kooi
Faculty of Earth and Life Sciences, Department of Theoretical Biology, Vrije Universiteit,
De Boelelaan 1085, Amsterdam 1081 HV, The Netherlands
e-mail: tineke@bio.vu.nl

U. Dieckmann
Evolution and Ecology Program, International Institute for Applied Systems Analysis, Schlossplatz 1,
Laxenburg 2361, Austria

example, whales feeding on plankton and hyena eating zebra. Like body size, prey-size preference is an important ecological property, as it determines which trophic links between predators and prey are established. Together, the body size and the prey-size preference of predators largely define the structure of a community. While the effects of body size on individuals and populations has been investigated from many angles (Peters 1983; Kooijman 1986; Yodzis and Innes 1992; Brown et al. 1993), general relationships between a predator's body size and its prey-size preference are more difficult to find.

Various mechanisms have been proposed that attempt to explain predator–prey size ratios and prey-size preferences. These include passive selection mechanisms such as prey visibility (Rincon and Loboncervia 1995; Svensson 1997) or gape limitation (Rincon and Loboncervia 1995; Forsman 1996; Mehner et al. 1998; Karpouzi and Stergiou 2003). Active selection mechanisms, on the other hand, underlie optimal foraging theory, which assumes that predators select prey sizes that provide the best energy returns. Several mechanisms based on active selection are discussed in Ellis and Gibson (1997), Manatunge and Aseada (1998), Rytkonen et al. (1998), Kristiansen et al. (2000), Tureson et al. (2002) and Husseman et al. (2003). However, since results vary both within and between predator–prey systems, and the found relationships are highly species-specific, it is difficult to extract general rules from them.

In recent years, several models have been developed that focus on general large-scale patterns of feeding links in food webs. Some of these models, such as the cascade model (Cohen and Newman 1985) and the niche model (Williams and Martinez 2000), are able to generate food webs that approximate many features observed in real food webs. However, these models are often descriptive and predator–prey pairs are assigned at random. Other models do have a more mechanistic basis and include physiological relations based on body size, but assume a fixed predator–prey size ratio (Loeuille and Loreau 2005). Aljetlawi et al. (2004) derived a functional response that accounts for both predator and prey size: the derived relation was sufficiently flexible to be adjusted to many different specific predator–prey systems. This very flexibility, however, limits the scope for deriving general rules.

In this study we combine a process-based eco-physiological model with a functional response that depends on the size of both predator and prey. The model is based on dynamic energy budget (DEB) theory (Kooijman 2000, 2001), a versatile framework for modeling metabolic processes with physiological rules for uptake and use of material and energy. DEB theory does not specify all details of the size-dependence of the functional response. One of our aims here is to make the terms underlying this functional response explicit and, where necessary, include additional terms, while staying as close to DEB theory as possible.

We do not arbitrarily choose predator–prey size ratios, but instead we allow the predator size and its prey-size preference to evolve independently. The predators are supplied with prey that have a range of sizes. To keep the analysis feasible, we assume that the size distribution of prey is constant and does not evolve. The objective is to study which size combinations between predators and preys are feasible and to which predator–prey size ratios the considered population or community will eventually evolve. More specifically, we study how patterns of predator size and prey-size preference depend on various factors, given a fixed prey-size distribution; the examined factors include environmental parameters and ecological parameters, with the latter describing predation as well as competition. The model focuses on a generalized predator with two life stages, and therefore is not intended to replace more species-specific studies on size-selective prey choice. By retaining a general perspective, we hope that the results reported below will

provide insights into the various factors determining predator–prey size ratios, and thereby will help understanding of predator–prey size patterns observed in nature.

Model description

Population dynamics

We consider a predator–prey model in which a population of predators feed on one or more populations of abiotic prey.

The predators are described by one state variable, their biomass density X_A (given by the total amount of structural biovolume per unit of system volume), and by two adaptive traits, their adult length ℓ_A and their preference for a prey length ℓ_P. These two adaptive traits remain constant throughout an individual's life, but may change from parent to offspring through mutation. Prey populations are described by their biomass density X_i, and consist of organisms of length ℓ_i, with $i = 1,\ldots, n$ where n is the number of prey populations. The prey populations are not interacting and are assumed to have a fixed size-structure. For example, we could consider algal populations grown in a first (illuminated) chemostat and fed into a second (dark) chemostat where they are consumed by rotifers (see Kooi and Kooijman 1999).

Our model for the predator is based on a model of a size-structured rotifer population (Kooi and Kooijman 1997, 1999), of which we use a simplified version that includes only two life stages for the predator, embryos and adults. Embryos do not feed, but grow by using the reserves they got from their mothers when eggs were produced. Adults, in contrast, do not grow but they do feed; the acquired energy is used for maintenance and egg production. Separating the functions of growth and feeding simplifies the model by reducing the number of equations. It also removes intraspecific body size scaling relations, but maintains interspecific scaling relations. These include a size-dependent egg-production period a_A and a size-dependent developmental period a_b of the embryo. A continuous function for reproduction then allows the system to be expressed in terms of delay differential equations (DDEs). The dynamics of the system can then be described as follows,

$$\frac{\mathrm{d}}{\mathrm{d}t}X_i(t) = (X_{r,i} - X_i(t))D - I_i f_i(t) X_A(t), \tag{1a}$$

$$\frac{\mathrm{d}}{\mathrm{d}t}X_A(t) = R(t - a_b)\exp(-h a_b) X_A(t - a_b) - h X_A(t), \tag{1b}$$

where $X_{r,i}$ is the incoming density of prey i, f_i is the predator's functional response to prey i (to be further discussed in Section "Functional responses"), I_i is the maximum volume-specific ingestion rate of prey i (which equals the inverse of the handling time $[t_{h,i}]$ multiplied by the probability ρ_s that an attack is successful, $I_i = \rho_s/[t_{h,i}]$, where the square brackets indicate that the handling time is expressed on a volume-specific basis), D is the dilution rate of prey, and h is the predator's mortality rate. The delay in reproduction $(t - a_b)$ is due to the predator's embryo development time a_b, which depends on how fast energy can be mobilized, as described by the specific energy conductance k_E, $a_b = 3/k_E$ (Kooi and Kooijman 1997). Embryos have the same mortality rate as adults, and the term $\exp(-h a_b)$ accounts for the mortality of embryos during their development. The predator's reproduction rate is given by

$$R(t) = \frac{h}{\exp(h a_A(t)) - 1}, \tag{2}$$

(Kooi and Kooijman 1997), which depends on the mortality rate h. Generally, reproduction rates do not depend directly on adult mortality, but the expression above accounts for the death of eggs during the egg-production period caused by the mortality of (egg-producing) mothers. For small mortality rates, the reproduction rate equals the inverse of the egg-production period, $R(t) = 1/a_A(t)$.

An expression for $a_A(t)$ was derived by Kooi and Kooijman (1997). Their expression is given by the ratio between the amount of energy needed per egg and the rate with which energy becomes available for reproduction. The latter depends on the scaled energy density e of the mother (i.e., on the volume-specific amount of energy $[E]$ divided by the maximum energy content $[E_{max}]$) and on the specific energy conductance k_E. At equilibrium, the scaled energy density e of an adult equals its scaled functional response f, so that the amount of mobilized energy equals $k_E f$. From this mobilized energy, first the costs of maintenance have to be paid, calculated by multiplying the maintenance rate coefficient k_M (ratio of costs for maintenance per unit of time to costs for growth) with the energy investment ratio g (the proportion of the total amount of available energy that is used for growth). The scaled energy density required to produce an egg depends on the costs for the structural biomass of a newborn individual and the costs for growth and maintenance during the embryonic period, $g^+ = g + \frac{3}{4} g k_M / k_E$ (Kooi and Kooijman 1997), as well as on the energy density of a newborn individual itself, $\hat{e}$. Based on these considerations, the egg-production period is obtained as

$$a_A(t) = \frac{g^+ + \hat{e}(t)}{k_E f(t) - k_M g}, \tag{3}$$

(Kooi and Kooijman 1997). For a more detailed explanation of the model, including derivations of a_b, R, a_A, and g^+, readers may want to consult the original work by Kooi and Kooijman (1997, 1999). All parameters and variables of the model are summarized in Table 1, with all default parameter values listed in Table 2.

Scaling considerations

Because this study considers adult length to be subject to evolution, some body-size scaling relations had to be included that were not taken into account in the original model (Kooi and Kooijman 1997, 1999), where body size was fixed. First, the energy investment ratio g was no longer assumed to be constant, but instead becomes dependent on body volume ℓ_{max}^3, following an expression central to DEB theory, $g = \upsilon/(k_M\, \ell_{max})$ (Kooijman 2000). Note that the adult body size ℓ_A of the predators is a fixed proportion α of their maximum size, $\ell_A = \alpha\, \ell_{max}$. This enables the model to cope with predators that quickly grow to adult size, without slowing down as would be expected from an asymptotic growth curve.

Second, the specific energy conductance k_E is equal to the energy conductance υ divided by the size of the organism, $k_E = \upsilon/\ell_A$. The rationale behind this scaling relation is that energy is mobilized across membranes, which have a surface area proportional to that of the organism. As a result, the developmental period of the embryo becomes dependent on adult body size as well, $a_b = 3\ell_A/\upsilon$. Third, the mortality rate h was assumed to scale with length, such that larger organisms have a longer life span, $h = D\ell_{ref}/\ell_A$; at the reference

Table 1 Parameters and state variables of the model

Symbol	Dimension	Meaning
Physiological parameters		
a_b, a_A	T	Embryo-development time and egg-production time; $a_b = 3/k_E$
e, $\hat{e}$	–	Scaled energy density, of adult and of newborn individuals; $e = [E]/[E_{max}] = f$
$[E]$, $[E_{max}]$, $[E_{max}]_{ref}$	EL^{-3}	Volume-specific energy density; actual, maximum, and reference
g, g^+	–	Energy investment ratio for biomass and embryo growth; $g^+ = g + \frac{3}{4}gk_M/v$
h	T^{-1}	Mortality rate
k_E	T^{-1}	Specific energy conductance; $k_E = v/\ell_A$
k_M	T^{-1}	Maintenance rate coefficient
R	T^{-1}	Reproduction rate
α	–	Proportion of the maximum size that is reached; $\alpha = \ell_A/\ell_{max}$
v	LT^{-1}	Energy conductance
Trophic parameters		
b, b_0	$l^3L^{-3}T^{-1}$	Volume-specific encounter rate and encounter rate coefficient
D	T^{-1}	Dilution rate
f, f_i	–	Functional response; overall, and with respect to prey population i
I_i	T^{-1}	Maximum volume-specific intake rate for prey population i
ℓ_i, ℓ_{max}, ℓ_{ref}	L	Length of individuals of prey population i; maximum length of predator; reference length
t_g, t_c, t_h	T	Ingestion, capture, and handling time
$[t_h]$, $[t_{h,i}]$, $[t_h]_{ref}$	T	Volume-specific handling time: actual, with respect to prey population i, and minimum
$[t_{g,0}]$, $[t_{c,\ 0}]$	T	Coefficients for volume-specific ingestion and capture time
$X_{r,i}$, $X_{r,0}$	L^3l^{-3}	Incoming prey density; function, and scaling coefficient
δ	L	Distance between the successive lengths of incoming prey-size distribution
μ	L	Mean length of incoming prey-size distribution
σ_P, σ	–	Standard deviation; of attack probability (niche width), and of incoming prey-size distribution
ρ_a, ρ_s	–	Attack probability and capture efficiency
Ecological state variables		
X_A, X_i	L^3l^{-3}	Structural volume density of (adult) predators and of prey population i
Evolutionary state variables		
ℓ_A	L	Adult length of predator
ℓ_P	L	Prey-size preference of predator

Dims: T, time; L, length of individual; l, length of reactor; E, energy

length ℓ_{ref} mortality rate h is equal to dilution rate D. As such, the dilution rate serves as a measure for the harshness of the environment.

The scaled energy density of the eggs $\hat{e}$ is assumed to depend on the scaled energy density e of the mother. In the original model (Kooi and Kooijman 1997, 1999), a mother would pass on to her eggs the precise amount of energy such that her offspring, after development and hatching, would have exactly the same energy density as herself. In this

Table 2 Default parameter values

Parameter	Default value
$\tilde{b}_0$	1000
$\tilde{D}$	0.1
$\tilde{\ell}_{\text{ref}}$	1
$[\tilde{t}_{\text{c},0}]$	3.5
$[\tilde{t}_{\text{g},0}]$	0.77
α	0.1
σ_{P}	0.05
σ	0.25
ρ_{s}	1
$\tilde{\mu}$	0.5

Tildes indicate that parameters are scaled by υ, k_{M} and/or $X_{\text{r},0}$ to make them dimensionless

way the mother proportioned the amount of energy per egg, while ensuring that her offspring would have sufficient energy at the start of its life (right after hatching), at least as long as the environment did not change in the meanwhile. Also, it implied that once the system had reached its equilibrium (with respect to prey, predator, and energy densities), it would remain exactly at this equilibrium (Alver et al. 2006). Here, however, we study the evolution of prey size-preference, and the offspring may encounter or prefer different prey sizes than its mother. Therefore, we assume here that a mother takes into account these uncertainties. She does so by providing her offspring not just with the amount of energy to end up after hatching with her own energy density $[E]$ she possesses, but with a larger energy density, $[\hat{E}]$, so that her offspring will always have sufficient energy densities after hatching, irrespective of the size of its prey. This is ensured when by scaling the energy density of eggs, not against the mother's own maximum energy density $[E_{\text{max}}]$ (which depends on prey-size availability for her), but against the maximum possible energy density $[E_{\text{max}}]_{\text{ref}}$. The corresponding scaled energy density $\hat{e}$ is given by

$$\hat{e} = \frac{[\hat{E}]}{[E_{\text{max}}]} = \frac{[\hat{E}]}{[E_{\text{max}}]_{\text{ref}}} \frac{[E_{\text{max}}]_{\text{ref}}}{[E_{\text{max}}]} = \frac{[E_{\text{max}}]_{\text{ref}}}{[E_{\text{max}}]} e. \tag{4a}$$

If we again use $e = f$, this can be rewritten as

$$\hat{e} = \frac{[E_{\text{max}}]_{\text{ref}}}{[E_{\text{max}}]} e = \frac{[E_{\text{max}}]_{\text{ref}}}{[E_{\text{max}}]} f = \frac{[t_{\text{h}}]}{[t_{\text{h}}]_{\text{ref}}} f, \tag{4b}$$

where the last step follows from the fact that the maximum energy density is proportional to the maximum ingestion rate, while the maximum ingestion rate is the inverse of the handling time, so that $[E_{\text{max}}] \propto 1/[t_{\text{h}}]$, (Kooijman 2000, p. 269).

Incoming prey densities

The model introduced above can be analyzed for one or more prey populations. In the latter case, the incoming prey densities $X_{\text{r},i}$ were assumed to vary gradually across prey populations, following a distribution with mean prey size μ, (dimensionless) standard deviation σ, and maximum density $X_{\text{r},0}$,

$$X_{\mathrm{r},i} = X_{\mathrm{r},0}\frac{\delta}{\sigma\sqrt{2\pi}}\exp\left(-\frac{1}{2}\frac{\ln(\ell_i/\mu)^2}{\sigma^2}\right), \tag{5}$$

where δ denotes the distance between the successive lengths of prey. For numerical purposes, this prey-size distribution was truncated at +3 and at −3 times the standard deviation σ, thus representing 98% of the total distribution. We found that a resolution of $n = 50$ was sufficient to ensure that results were essentially unaffected by discretization of the prey-size distribution.

Functional responses

The sequence of capturing a prey consists of encounter, attack, and handling. These interactions between predator and prey are assumed to follow a Holling type-II functional response,

$$f = \sum_{i=1}^{n} f_i, \quad \text{with} \quad f_i = \frac{X_i/K_i}{1 + \sum_{j=1}^{n} X_j/K_j} \quad \text{and} \quad 1/K_i = \rho_{a,i} b_i [t_{\mathrm{h},i}], \tag{6}$$

where K_i is the half-saturation constant of the functional response to prey i, b_i is the volume-specific encounter rate of the predator with prey i, $\rho_{a,i}$ is the attack probability for prey i, and $[t_{\mathrm{h}},i]$ is the volume-specific time required for handling prey i. These terms and their dependencies on the body sizes of both predator and prey, ℓ_{A} and ℓ_i, as well as on the prey-size preference of the predator, ℓ_{P}, are discussed below. In line with DEB theory, we base these relationships on general scaling principles involving the lengths ℓ, surface areas ℓ^2, or volumes ℓ^3 of the considered organisms. As a result, the relations derived here are less detailed than the relations derived by, e.g., Aljetlawi et al. (2004); our assumption below of fixed scaling exponents also avoids problems with varying dimensions, and thus interpretations, of scaling coefficients.

Encounter rate b

The encounter rate b_i of a predator with a prey of size ℓ_i arises from encounters within the predator's search area. This search area is assumed to be proportional to the predator's surface area, $b \propto \ell_{\mathrm{A}}^2$, as is the case, for instance, for sessile filter feeders that orient their arms perpendicular to the current. For filter feeders that generate their own current, the encounter rate equals the filter rate. Their flapping or beating frequency is observed to be independent of their size (Kooijman 2000), such that the generated current is proportional to the surface area of their extremities, and thus again to their surface area. Other organisms may lay in ambush and capture prey that come within reach, i.e., within a distance that is proportional to the length of a leg or jaw or tongue, such that also here the encounter rate scales with surface area. Mobile organisms generally move with a speed proportional to their length: if the width of the path searched for food is proportional to length, this again leads to an encounter rate that scales with surface area. The encounter rate also scales with the surface area of the prey ℓ_i^2, as the prey's visibility or detectability is assumed to be proportional to the prey cross-sectional area or silhouette. In summary, we assume $b_i \propto \ell_{\mathrm{A}}^2 \ell_i^2$. Because the population dynamics above were expressed on a

per-volume basis, b_i is divided by the volumes of predator and prey, leading to the following relationship,

$$b_i = b_0 \frac{\ell_{\text{ref}}^2}{\ell_{\text{A}} \ell_i}, \tag{7}$$

where the lengths are measured relative to a reference length ℓ_{ref}, so that the encounter rate coefficient b_0, which controls the absolute value of the encounter rate, has the same dimensions as b_i. Without any loss of generality, reference lengths were taken as equal for predator and prey.

Attack probability ρ_a

The predator prey-size preference ℓ_{P} is assumed to evolve separately from the predator's adult body size ℓ_{A} and is not imposed by morphological constraints such as limited gape size. Even though such structural limits may exist, we assume here that they are adjusted to the prey-size preference, rather than vice versa. The probability ρ_{a} with which a predator attacks a prey of size ℓ_i is assumed to be log-normally distributed and depends on the prey-size preference ℓ_{P} and (dimensionless) niche width σ_{P},

$$\rho_{a,i} = \exp\left(-\frac{1}{2} \frac{\ln(\ell_i/\ell_{\text{P}})^2}{\sigma_{\text{P}}^2} \right). \tag{8}$$

On encounter, a prey exactly of the preferred size ℓ_{P} will thus be attacked with certainty.

Handling time t_h

In general, the time required for handling each prey item comprises the time needed for capture and ingestion.

Ingestion is the process by which the prey is physically taken up into the body of the predator, passing through, for instance, its outer membrane or its gut wall. First of all, ingestion time t_{g} is assumed to be proportional to the amount of prey biomass that has to be ingested, and thus, for one prey individual, proportional to the prey volume, $t_{\text{g},i} \propto \ell_i^3$.

In addition, for *intra*specific comparisons, DEB theory assumes the ingestion time to be inversely proportional to the surface area through which the intake occurs, and this surface area is assumed to scale with the total surface area ℓ_{A}^2 of the predator. For small individuals, which have a favorable ratio between surface area and volume, the ingestion time thus is small, while for larger individuals, it is large. In this study, however, we assume all adult individuals of a population to have the same size, ℓ_{A}. For *inter*specific comparisons, DEB theory assumes ingestion rates to be proportional to maximum length, $\ell_{\max}$, which implies that $t_{\text{g}} \propto \ell_{\max}^{-1}$. Such a scaling may, for instance, be related to gut capacity (body plan) or diet composition of the predator.

Capture time is assumed to depend on the relative sizes of predator and prey. Larger prey require a longer capture time because they may be better protected, resist more strongly, or have to be cut into chunks before being ingested. Specifically, we assume that the capture time increases faster with prey size than does the corresponding yield, which

implies that it is proportional to size with an exponent larger than 3; as a default, here, we assume an exponent of 4, $t_c \propto (\ell_i/\ell_A)^4$.

The total handling time t_h equals the mean length of the handling process, consisting of capture and ingestion,

$$\begin{aligned} t_{h,i} &= t_{c,i} + \rho_s t_{g,i} \\ &= t_{c,0}\left(\frac{\ell_i}{\ell_A}\right)^4 + \rho_s \frac{t_{g,0}}{\ell_{max}} \frac{\ell_i^3}{\ell_A^2}, \end{aligned} \tag{9}$$

where $t_{g,0}$ and $t_{c,0}$ are the ingestion and capture coefficients, and ρ_s is the fraction of attacked prey that is actually captured; only this fraction has to be ingested. As a default, all attacks are assumed to be successful, $\rho_s = 1$; the effects of reduced capture efficiencies are studied in Section "Evolutionary effects of feeding modes".

Because adult size increases with maximum size, and since all adult organisms are assumed to possess adult size, ℓ_{max} can be substituted with ℓ_A/α. The time $t_{h,i}$ that a predator needs for handling an individual of prey i can be converted into the volume-specific handling time $[t_{h,i}]$, which measures the time that a volume-unit of predator needs for handling a volume-unit of prey i, through multiplication with $(\ell_A/\ell_i)^3$,

$$[t_{h,i}] = [t_{c,0}]\frac{\ell_i}{\ell_A} + \rho_s \alpha [t_{g,0}]. \tag{10}$$

The total handling time $[t_h]$ given the actual prey-size availability is the sum of prey-size specific handling times $[t_{h,i}]$ weighted with the fraction θ_i of all attacks that are directed at prey i,

$$[t_h] = \sum_{i=1}^{n} \theta_i [t_{h,i}], \quad \text{with} \quad \theta_i = \frac{\rho_{a,i} b_i X_i}{\sum_{j=1}^{n} \rho_{a,j} b_j X_j}. \tag{11}$$

Finally, $[t_h]_{ref}$ in Eq. 4b is the absolute minimum, or reference, handling time, which equals $[t_{h,i}]$ at infinitely small prey-sizes, $[t_h]_{ref} = [t_{h,i}]|_{\ell_i=0} = \rho_s \alpha [t_{g,0}]$, and thus only depends on predator size.

Choice of units

The model presented above was scaled by maintenance rate k_M, energy conductance υ, and incoming prey density coefficient $X_{r,0}$. Scaling renders the outcomes independent of these parameters. The unit of time, T, is chosen as k_M^{-1}, the unit of predator and prey length, L, is chosen as υ/k_M, and the unit of reactor length, l, is chosen as $\sqrt[3]{X_{r,0}}k_M/u$; the latter unit, however, only features in the dimensions of biomass-volume densities, $L^3 l^{-3}$, which are made dimensionless simply through division by $X_{r,0}$.

The remaining variables and parameters, which then become dimensionless, are denoted by a tilde: for instance, the predator size ℓ_A (dim: L) was divided by ν (dim: LT^{-1}) and multiplied by k_M (dim: T^{-1}) so that the scaled length $\tilde{\ell}_A$ is dimensionless. The scaled predator and prey densities are indicated by x instead of X, e.g., $x_A = X_A/X_{r,0}$, and the scaled time t is indicated by τ. The default values of the scaled parameters are shown in Table 2. The scaled model can thus be written as follows,

$$\frac{\mathrm{d}x_i}{\mathrm{d}\tau} = (x_{r,i} - x_i)\tilde{D} - \tilde{I}_i f_i x_\mathrm{A}(\tau), \tag{12a}$$

$$\frac{\mathrm{d}x_\mathrm{A}}{\mathrm{d}\tau} = \tilde{R}(\tau - \tilde{a}_b)\exp(-\tilde{h}\tilde{a}_b)x_\mathrm{A}(\tau - \tilde{a}_b) - \tilde{h}x_\mathrm{A}(\tau). \tag{12b}$$

The scaled reproduction rate $\tilde{R}$ is given by

$$\tilde{R}(\tau) = \frac{\tilde{h}}{\exp(\tilde{h}(g^+ + \hat{e}(\tau))(f(\tau)/\tilde{\ell}_\mathrm{A} - g)^{-1}) - 1}, \tag{13}$$

where f is the functional response, as given in Eq. 6, and $\hat{e}$ is the scaled energy density of an egg, as given in Eq. 4. Furthermore, $\tilde{D}$ is the scaled dilution rate, $\tilde{h} = \tilde{D}\tilde{\ell}_\mathrm{ref}/\tilde{\ell}_\mathrm{A}$ is the mortality rate, $\tilde{a}_b = 3\tilde{\ell}_\mathrm{A}$ is the scaled egg development rate, g is the energy investment ratio, $g = \alpha/\tilde{\ell}_\mathrm{A}$, and $g^+ = g + \frac{3}{4}\alpha$ is the difference in reserve density between the beginning and end of egg development. Note that f, g, and $\hat{e}$ already were dimensionless variables before, and are therefore not affected by any choice of units.

Methods

Ecological analysis

The coexistence set is the region in the trait space of the predator's body size $\tilde{\ell}_\mathrm{A}$ and its prey-size preference $\tilde{\ell}_\mathrm{P}$ in which the predator and prey populations can coexist, i.e., where $x_i^* > 0$ for $i = 1,\ldots, n$ and $x_\mathrm{A}^* > 0$. Here and below, a superscripted asterisk indicates a population equilibrium, e.g., the scaled reproduction rate at equilibrium is denoted by $\tilde{R}^*$. At each point of this trait space there also exists a boundary equilibrium, $x_\mathrm{A}^* = 0$ and $x_i^* = x_{r,i}$, which is unstable for trait combinations within the coexistence set and stable for those outside. In other words, the boundary of the coexistence set is formed by trait combinations for which the boundary equilibrium changes stability. Consequently, only within the coexistence set there is a positive equilibrium of the prey–predator system. The resulting figure (Fig. 1) showing the coexistence set is explained in more detail in Section "Results/Ecological analysis".

We restrict the discussion of the coexistence set to the case in which a single prey population is supplied to the system. This enables us to check whether a predator can coexist with prey of a specific size, without this being influenced by the precise choice of niche width or prey-size distribution. Accordingly, we assume that the prey-size preference of the predator matches exactly the one available prey size, $\tilde{\ell}_\mathrm{P} = \tilde{\ell}_1$. This cuts short the evolution of prey-size preference, which will evolve to the size of the available prey anyway (as this is the only one available). The resulting coexistence set will thus show which predators can live on which prey. More precisely, the set shows whether a predator of certain size can coexist with a prey of a certain size when these prey are of the predator's preferred size.

An equilibrium point on the boundary of the coexistence set is given by $(\tilde{\ell}_\mathrm{A}, \tilde{\ell}_\mathrm{P} = \tilde{\ell}_1)$ for which $x_1^* = x_{r,1}$, $x_\mathrm{A}^* = 0$, and $\tilde{R}^*\exp(-\tilde{h}\tilde{a}_b) = \tilde{h}$, where $\tilde{R}^*$ is the equilibrium value of $\tilde{R}$ in Eq. 13. The remaining points $(\tilde{\ell}_\mathrm{A}, \tilde{\ell}_\mathrm{P} = \tilde{\ell}_1)$ on the boundary of the coexistence set were then determined by numerically continuating this condition using standard continuation software.

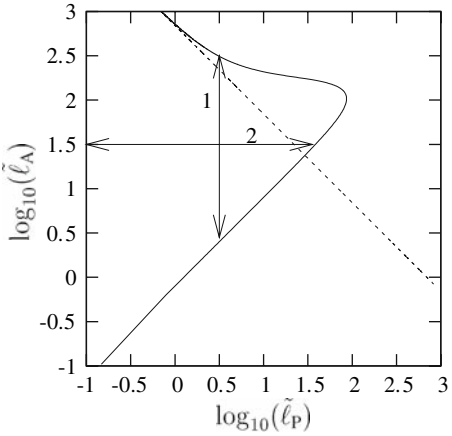

Fig. 1 Coexistence set of the investigated predator–prey system. Combinations of scaled predator body size $\tilde{\ell}_A$ (vertical) and prey-size preference $\tilde{\ell}_P$ (horizontal) are shown logarithmically, assuming that the preferred prey size equals the one available prey size ($\tilde{\ell}_P = \tilde{\ell}_1$). The dashed curve depicts the boundary of this coexistence set when only ingestion and encounter times are considered, while the continuous curve shows this boundary when capture times are considered as well. The two arrows indicate the graph's two possible interpretations: (1) the feasible range of predator body sizes for a given prey size, and (2) the feasible range of prey-size preferences for a given predator size

Adaptive dynamics theory

For the evolutionary analysis of our model we utilized adaptive dynamics theory, a general framework that helps investigate phenotypic evolution under frequency-dependent selection (Dieckmann and Law 1996; Metz et al. 1996; Dieckmann 1997; Geritz et al. 1997). This approach assumes a time scale separation between the ecological and evolutionary dynamics, so that mutations in adaptive traits occur sufficiently rarely for the considered resident population always to be close to its population dynamical equilibrium when probed by a mutant. Mutants with a positive invasion fitness may replace the resident population. A series of such replacements leads to phenotypic change of the population. The directions and endpoints of phenotypic change depend on the selection gradient and are calculated by means of the so-called canonical equation of adaptive dynamics (Dieckmann and Law 1996). Below we specify, in turn, these general notions for the model analyzed in this study.

Invasion fitness

The invasion fitness of a mutant is defined by its long-term per capita growth rate $r(\tilde{\ell}_m, E_r(\tilde{\ell}_r))$ while being rare in the environment E_r set by the resident population at its ecological equilibrium. Here, $\tilde{\ell}$ is the vector of the predator's adaptive traits $\tilde{\ell} = (\tilde{\ell}_A, \tilde{\ell}_P)$ and the subscripts 'r' and 'm' indicate resident and mutant trait values, respectively. To calculate the invasion fitness of the mutant we extend Eq. 12 by including the dynamics of the mutant predator,

$$\frac{dx_{A,m}}{d\tau} = \tilde{R}_m(\tau - \tilde{a}_{b,m}) \exp(-\tilde{h}_m \tilde{a}_{b,m}) x_{A,m}(\tau - \tilde{a}_b) - \tilde{h}_m x_{A,m}(\tau). \tag{14}$$

Introducing a mutant in the system also requires a feeding term to be added to Eq. 12a, as shown in Eq. 21.

As explained in detail in the appendix (Eq. 31), the invasion fitness of the mutant is thus given by

$$s(\tilde{\ell}_{\mathrm{m}}, \tilde{\ell}_{\mathrm{r}}) = \tilde{R}^{*}_{\mathrm{m}} \exp(-\tilde{h}_{\mathrm{m}} \tilde{a}_{\mathrm{b,m}}) - \tilde{h}_{\mathrm{m}}, \tag{15}$$

where $\tilde{R}^{*}_{\mathrm{m}}$ is the mutant's reproduction rate at the system's equilibrium,

$$\tilde{R}^{*}_{\mathrm{m}} = \frac{\tilde{h}_{\mathrm{m}}}{\exp(\tilde{h}_{\mathrm{m}}(g^{+}_{\mathrm{m}} + \hat{e}_{\mathrm{m}})/(f_{\mathrm{m}}/\tilde{\ell}_{\mathrm{A,m}} - g_{\mathrm{m}})) - 1}. \tag{16}$$

Here the functional response f_{m} of the mutant depends on the adaptive traits of both mutant and resident, because the resident predator sets the environment E_{r} and thus determines the equilibrium prey density in the system.

Selection gradient

The expected direction of phenotypic change is proportional to the selection gradient, i.e., to the derivative of invasion fitness with respect to the adaptive traits of the mutant, evaluated at the trait values of the resident. For a monomorphic resident population, this selection gradient is denoted by

$$\nabla_{\mathrm{m}} s(\tilde{\ell}_{\mathrm{m}}, \tilde{\ell}_{\mathrm{r}}) = \left(\frac{\partial}{\partial \tilde{\ell}_{\mathrm{A,m}}} s(\tilde{\ell}_{\mathrm{m}}, \tilde{\ell}_{\mathrm{r}}), \frac{\partial}{\partial \tilde{\ell}_{\mathrm{P,m}}} s(\tilde{\ell}_{\mathrm{m}}, \tilde{\ell}_{\mathrm{r}}) \right) \Bigg|_{\tilde{\ell}_{\mathrm{m}} = \tilde{\ell}_{\mathrm{r}}}. \tag{17}$$

Canonical equation

A deterministic approximation of the stochastic evolutionary trajectories of body size and prey-size preference, jointly driven by mutation and selection, is provided by the canonical equation of adaptive dynamics (Dieckmann and Law 1996), which for our system is given by

$$\frac{\mathrm{d}\tilde{\ell}_{\mathrm{r}}}{\mathrm{d}t} = \rho(\tilde{\ell}_{\mathrm{r}}) \frac{x^{*}_{\mathrm{A,r}}}{\tilde{\ell}^{3}_{\mathrm{A,r}}} \nabla_{\mathrm{m}} s(\tilde{\ell}_{\mathrm{m}}, \tilde{\ell}_{\mathrm{r}}). \tag{18}$$

Here ρ is a compound parameter consisting of the product of the 2×2 variance-covariance matrix of the multivariate mutation distribution (Dieckmann and Law 1996), the factor 1/2, the mutation probability, and the coefficient of variation of clutch sizes. As mutations in the two predator traits are assumed to be independent, the variance-covariance matrix of the mutation distribution is a diagonal matrix. The value of ρ is irrelevant for this study as we are only interested in evolutionary equilibria, and not in the timing of the trajectories leading towards them.

Evolutionary outcomes

Eventually, the population will reach a combination of trait values $\tilde{\ell}_{\mathrm{r}}$ at which the selection gradient vanishes,

$$\nabla_{\mathrm{m}} s(\tilde{\ell}_{\mathrm{m}}, \tilde{\ell}_{\mathrm{r}}) = 0. \tag{19}$$

Such an evolutionary equilibrium may be either stable or unstable according to Eq. 18. An evolutionary equilibrium may also be situated at a fitness maximum, a fitness minimum, or a fitness saddle according to Eq. 15. In the latter two cases, the evolutionary equilibrium is not locally evolutionarily stable, so that the resident population may split up and evolve into two or more sub populations through a process known as evolutionary branching (Metz et al. 1992, 1996; Geritz 1997, 1998).

Evolutionary analysis

Single-trait evolution

As a preparatory step in the evolutionary analysis of our model, we focus on the evolution of the predator's body size. For this purpose we assumed, like in the ecological analysis, that only a single prey population exists and that the predator's prey-size preference always matches this prey size, $\tilde{\ell}_{\mathrm{P}} = \tilde{\ell}_{1}$. In this case, the evolutionary dynamics are reduced to the single trait $\tilde{\ell}_{\mathrm{A}}$. The evolutionary outcome of $\tilde{\ell}_{\mathrm{A}}$ represents the body size towards which a predator will evolve when feeding on prey of a certain size. This evolutionary body size was found numerically by integrating the dynamics of $\tilde{\ell}_{\mathrm{A}}$ according to the canonical equation of adaptive dynamics, Eq. 18, while keeping $\tilde{\ell}_{\mathrm{P}}$ and $\tilde{\ell}_{1}$ fixed, until an evolutionary equilibrium was reached. This evolutionary equilibrium was then determined for a range of prey sizes (and thus prey-size preferences) within the coexistence set.

Two-trait evolution

The full evolutionary dynamics were studied by allowing the two adaptive traits of the predator to evolve jointly. In this case, a range of prey sizes was assumed to be available to the predator according to Eq. 5. The evolutionary equilibrium was again found numerically, by integrating Eq. 18.

Evolutionary branching

To study the evolutionary process after an evolutionary equilibrium had been reached, an extended numerical analysis was carried out. This analysis consisted of first integrating Eq. 18 until reaching an evolutionary equilibrium. If this equilibrium was evolutionarily unstable, i.e., if it corresponded to a fitness minimum or fitness saddle, the original predator population was equally split into two predator populations and the two corresponding canonical equations were considered further. The trait values of the two predator populations were chosen to deviate slightly from that of their ancestor in the two (opposite) directions of highest fitness increase around the ancestral combination of trait values. The two canonical equations were integrated, and new predator populations were added analogously if applicable, until a locally evolutionarily stable evolutionary equilibrium was reached, corresponding to a fitness maximum in all predator populations. Due to the

deterministic nature of the adaptive dynamics, more than one predator population may branch at the same time.

Mutual predation

Finally, to explore the effects of predation among predators, the functional response f was calculated as the sum of partial functional responses f_i, where i now consisted of all prey populations ($i = 1,\ldots, n$) as well as of all predator populations ($i = n + 1,\ldots, p$),

$$f = \sum_{i=1}^{n+p} f_i. \tag{20}$$

Stochastic evolution

As a further robustness test, we used a stochastic simulation process instead of the deterministic dynamics in Eq. 18. Underlying equations were adjusted for multiple prey populations as discussed at the end of the appendix. We repeatedly integrated the ecological dynamics of the system for 10^4 time steps, followed by the addition of a new mutant predator population to the system. The trait values of the mutant were drawn at random from a normal distribution around the trait values of its ancestor with a standard deviation of 10^{-3}. The initial biomass of the mutant population was set to a very small value, $x_{\mathrm{A,m}} = 10^{-20}$. This value was also used as the cutoff biomass density below which a population was assumed to go extinct. In the case of extinction, the affected population was removed from the system.

Results

Ecological analysis

We start by studying which predator–prey size combinations can coexist. As explained above, we restrict the analysis of the coexistence set to the case in which a single prey population is supplied to the system. For this analysis, the predator's prey-size preference equals the single available prey size assumed to be available, $\tilde{\ell}_{\mathrm{P}} = \tilde{\ell}_1$. The resultant coexistence set is shown in Fig. 1. This figure can be interpreted in two ways: vertically, as the feasible range of predator body sizes for a given prey size (illustrated by arrow 1), and horizontally, as the feasible range of prey-size preferences for a given predator body size (illustrated by arrow 2).

We separately determined the coexistence set for two different functional responses. First, only the basic handling processes of encountering and ingesting prey were assumed to play a role in the functional response of the predator ($[\tilde{t}_{\mathrm{c},0}] = 0$, for other parameter values see Table 2). In this case, Fig. 1 shows that the maximum feasible predator body size is inversely related to the maximum feasible prey size (dashed line). Second, the model was extended by including a capture time that depends on the predator–prey size ratio. Now, large predator–prey size ratios are no longer feasible, and the boundary of the coexistence set becomes curvilinear (continuous curve).

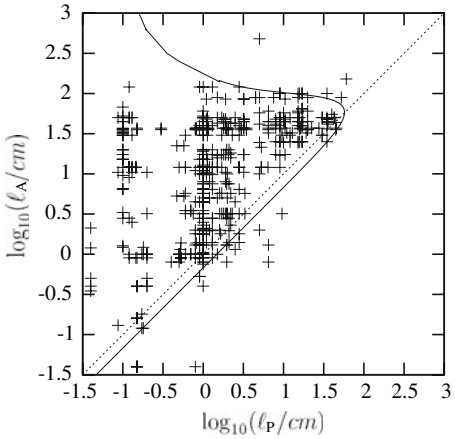

Fig. 2 Comparison of the coexistence set predicted by our model (continuous curve) with empirical data presented by Cohen et al. (1993). The logarithm of the length of the predator is plotted against the logarithm of the length of the prey, with both lengths being expressed in centimeters. Along the dotted line, body sizes of prey and predator are equal. The dimensionless variables $\tilde{\ell}_A$ and $\tilde{\ell}_P$ were translated back into lengths using the two relevant scaling parameters, $k_M = 1.44\ d^{-1}$ and $\upsilon = 0.3\ cm\ d^{-1}$; the dilution rate was set to $\tilde{D} = 0.05$

Figure 2 shows a set of empirically observed combinations of predator–prey sizes that were presented by Cohen et al. (1993), together with the coexistence set of our model based on a size-ratio-dependent capture time (continuous curve). The empirical dataset consists of 478 size combinations from 30 food webs. In the doubly logarithmic plot, these are distributed over a triangular area that is bounded above by a maximum predator size, bounded below by the equality of predator and prey sizes, and bounded on the left by the minimum prey size. The coexistence sets in Figs. 1 and 2 (continuous curves) are identical, but for Figure 2 the length variables are translated back from dimensionless variables into lengths expressed in centimeters. For the two relevant scaling parameters, k_M and υ, reasonable values were chosen that lie well within the range of empirically observed values ($k_M = 1.44\ d^{-1}$, $\upsilon = 0.3\ cm\ d^{-1}$; Kooijman 2000); the dilution rate was adjusted $(\tilde{D} = 0.05)$ so as to obtain a slightly better fit for the upper boundary of the coexistence set.

Evolutionary analysis

After having established which combinations of a predator's body size and its prey-size preference are ecologically feasible, we also studied the evolutionary dynamics of these adaptive traits. Figure 3 again shows the coexistence set (continuous curve) and the diagonal along which predator size and prey-size preference are equal (dotted line). The dashed line shows the body size to which the predator will evolve when feeding on a prey of a given size. In other words, it shows how the evolutionary equilibrium depends on prey size. This line results from single-trait evolution in ℓ_A, and applies when only one prey size is available and $\tilde{\ell}_P = \tilde{\ell}_1$. The figure shows that the evolved predator size is positively correlated with prey size, and that the slope of the correlation line is equal to unity.

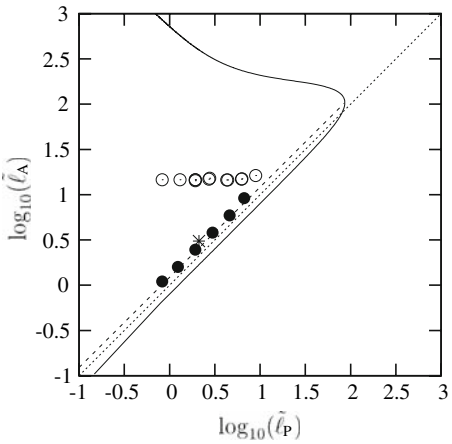

Fig. 3 Evolutionary outcomes of scaled predator body size $\tilde{\ell}_A$ and prey-size preference $\tilde{\ell}_P$. The continuous curve depicts the boundary of the coexistence set, while the dotted line depicts the diagonal along which predator size and prey-size preference are equal. The dashed line shows the outcome of single-trait predator evolution in $\tilde{\ell}_A$, for a single prey size, with $\tilde{\ell}_P = \tilde{\ell}_1$. The asterisk indicates the initial evolutionary equilibrium (and primary evolutionary branching point) of two-trait evolution in the predator when considering a range of available prey sizes. The filled circles show the composition of the predator community after evolutionary branching (deterministic evolution), while the open circles depict this composition when predation among predators was also taken into account (stochastic evolution)

When, instead of one prey size, a range of prey sizes is available simultaneously to the predator, as described in Section "Incoming prey densities", and both traits are allowed to evolve jointly, the predator population evolves to an evolutionary equilibrium within the coexistence set, which in Fig. 3 is denoted by an asterisk.

However, after this evolutionary equilibrium is reached, evolution continues. Since the evolutionary equilibrium does not correspond to an evolutionarily stable fitness maximum, the originally monomorphic predator population splits up into two populations and thus becomes dimorphic. This process of evolutionary branching is repeated several times, such that the predator population cascades into a range of populations with different trait combinations, until a locally evolutionarily stable predator community is eventually reached. In Fig. 3 the trait combinations realized in this evolved community are shown by filled circles.

Inclusion of predation among predators also leads to sequential evolutionary branching. The trait combinations resulting under stochastic evolution after 5000 mutations are shown in as open circles in Fig. 3; at this point in time the system is close to a locally evolutionarily stable equilibrium. The slightly irregular spacing of the realized trait combinations reflects the stochastic nature of the evolutionary process.

Figure 4 shows how the predator's body size and prey-size preference at the initial evolutionary equilibrium (i.e., before the first evolutionary branching) are affected by the availability of prey sizes. Specifically, the three panels show how the predator's adaptive traits vary with three features of the prey: the mean $\tilde{\mu}$ and standard deviation σ of the prey-size distribution, and the prey's dilution rate $\tilde{D}$. Analogously, Fig. 5 shows the variation of the predator's adaptive traits with two features of the predator: its niche width σ_P and its probability ρ_s of successfully capturing an attacked prey.

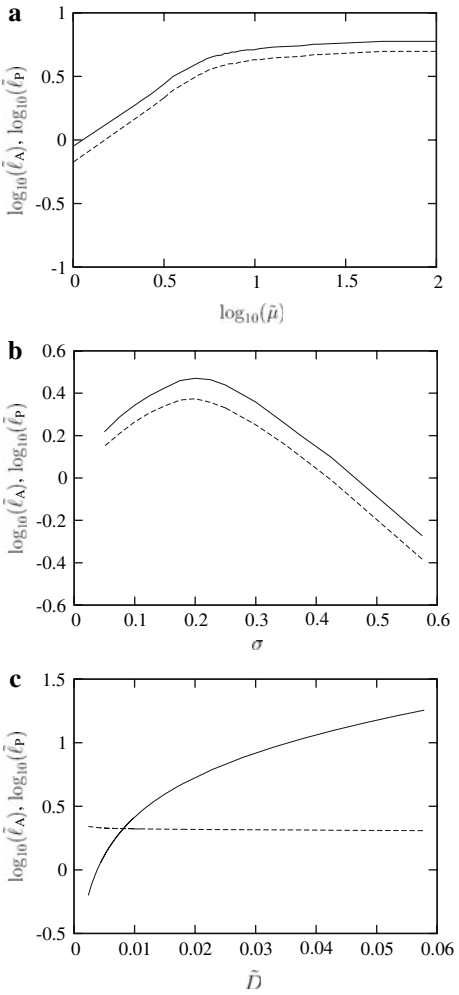

Fig. 4 Effects of environmental parameters on the evolutionary outcomes of scaled predator body size $\tilde{\ell}_A$ (continuous curve) and prey-size preference $\tilde{\ell}_P$ (dashed curve). The three panels show the evolutionary equilibrium values (**a**) for a range of means $\tilde{\mu}$ of the available prey-size distribution, (**b**) for a range of standard deviations σ of this distribution, and (**c**) for a range of dilution rates $\tilde{D}$

Discussion

In the first two subsections below we discuss the results of our ecological analysis, followed by three subsections of discussion on the results of our evolutionary analysis.

True predators versus parasitic predators

When taking into account only the basic handling processes of encountering and ingesting of prey, small predator–prey size ratios are feasible (Fig. 1, dashed line). Clearly, this does not agree with the distribution of empirically observed predator–prey sizes shown in Fig. 2. However, small size ratios are typically found in parasite-host systems (Memmott et al. 2000), which were not included in the empirical dataset of Cohen et al. (1993). Parasites are organisms that obtain their nutrients from one or very few host individuals, causing harm but no (immediate) death. True predators, in contrast, continuously require new prey

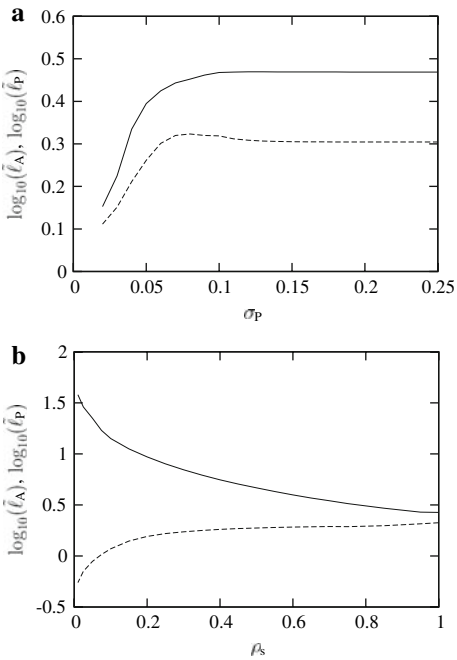

Fig. 5 Effects of ecological parameters on the evolutionary outcomes of scaled predator body size $\tilde{\ell}_A$ (continuous curve) and prey-size preference $\tilde{\ell}_P$ (dashed curve). The two panels show the evolutionary equilibrium values (**a**) for a range of niche widths σ_P and (**b**) for a range of capture efficiencies ρ_s

individuals, which are killed at attack or quickly thereafter. Because parasites do not have to overpower their prey, capture times may be neglected. Under these circumstances, our model predicts that small predator–prey size ratios are feasible, in qualitative agreement with empirical data.

The transition between parasites and true predators, however, is gradual. This is illustrated by the typical classification of a bird-egg eating snake as a predator, while the sea-cucumber-egg eating pearl fish is classified as a parasite. Examples from the wide range of parasitic relationships are discussed by Combes (2001). Whatever classification rules are defined, many exceptions can be found, pointing to the fact that these boundaries are essentially artificial. DEB theory assumes that predators and parasites are basically of the same kind, and only differ physiologically. The resulting differences in their parameter values, however, may lead to considerable, even qualitative, differences in the feasibility of predator–prey size combinations. In the results of our model, this is reflected by the qualitative change in the shape of the coexistence set when capture times are considered (Fig. 1, continuous curve). In this case, the coexistence set is shrunk and it is no longer feasible for small predators to feed on large prey.

Hence, by adjusting capture times in our model (e.g., by varying the capture time coefficient), we can account for both parasites and true predators. Similarly, by adjusting other parameter values, our model may also be expected to account for other types of predators, such as grazers or parasitoids. As a default, however, we considered a capture time coefficient that is relatively large, implying that the model mainly corresponds to true predators.

Imperfect upper triangularity

When including in our model a capture time that depends on the predator–prey size ratio, the feasible set becomes triangularly shaped (Fig. 1, continuous curve), which matches the

empirical distribution of observed predator–prey size combinations presented by Cohen et al. (1993) (Fig. 2). This so-called 'upper triangularity' is often found in real food webs (Warren and Lawton 1987; Cohen at al. 1993, 2003). The term stems from considering a food web's matrix of trophic interaction coefficients, in which species are arranged in hierarchical order, such that all of the non-zero matrix elements lie above the main diagonal. In the present study, the emergence of upper triangularity implies that larger predators can feed on a wider range of prey sizes and that for smaller prey sizes, the feasible range of predator sizes is wider. It also implies that a given species essentially does not eat other species that are larger than itself, which suggests a body-size-based hierarchy. Body size has been suggested previously to provide a mechanistic interpretation for the hierarchy assumption in the cascade model (Cohen and Newman 1985), both by Warren and Lawton (1987) and by Cohen (1989). However, in our analysis we did not postulate a size hierarchy as such: instead, this hierarchy naturally emerges from the scaling relations and size-dependent functional response suggested by DEB theory, and in particular from the considered proportionality of capture time to predator–prey size ratio.

The value of the capture time coefficient $[\tilde{t}_{c,0}]$ considerably affects the shape of the coexistence set. Yet, when plotted on a doubly logarithmic scale, different values of $[\tilde{t}_{c,0}]$ all result in a lower boundary of the coexistence set given by a straight line with slope one, corresponding to a fixed predator–prey size ratio. Although these lines have different intercepts, they lie rather close to each other and to the main diagonal for a relatively large range of values for $[\tilde{t}_{c,0}]$, especially when large predator and prey size ranges are considered. This finding would explain why, across many natural systems, the distribution of body size combinations involved in predator–prey links seems to be essentially the same.

Although the predicted boundaries of the coexistence set fit the empirical data reasonably, the fit is not perfect. For example, part of the predicted curvilinear upper boundary of the coexistence set, corresponding to combinations of small prey sizes with large predator sizes, is not observed in the considered empirical dataset. Instead, the upper boundary in the empirical dataset may be described simply by the body size of predators maxing out at about 150–200 cm. In the model, this curvilinear upper boundary is mainly determined by the encounter rate between predator and prey being proportional to the prey's surface area. Apparently, in natural systems, this is not realistic for large predators in combination with small prey. Probably, at these size ratios, the prey is not detected by vision, and the detectability may not be proportional to a prey's silhouette. This implies that the model's fit in this range of size combinations could be improved by including additional mechanisms. However, we chose to keep our model simple and to stay in line with DEB theory by including as few additional assumptions as possible.

An interesting property of the model is that the predicted lower boundary of the predicted coexistence set (Fig. 2, continuous curve) does not coincide with the diagonal along which predator and prey sizes are equal (dotted line), but instead lies below it (as discussed above, the exact location of this lower boundary depends on parameter values, and especially on the capture time coefficient $[\tilde{t}_{c,0}]$). The coexistence set thus extends to predators feeding on prey individuals that are larger than themselves.

Cohen et al. (1993) found that, in their dataset, approximately 10% of all predators fed on larger prey. Empirical studies have demonstrated this effect also for other natural food webs. Because of these consistent observations, the simple cascade model (Cohen and Newman 1985) has been extended, resulting in the more general niche model (Williams and Martinez 2000), which is viewed as providing better matches with empirical food web data (Warren and Lawton 1987; Neubert et al. 2000; Cohen et al. 2003). The proposed explanations are all based on the assumption that a certain hierarchy exists, but that the

measures or variables used to characterize it may be imperfect. In contrast, the size-ratio-dependent capture time assumed in our model provides a mechanism that naturally explains a body-size-based hierarchy while also allowing for 'exceptional' predator–prey links. This result suggests that not the measures or the variables, but rather the hierarchy itself is imperfect.

Predator evolution under increased levels of ecological realism

Our approach allows us to study and disentangle the evolutionary effects caused by the successive incorporation into our model of increased levels of ecological realism. Five such steps have been taken. First, we started out from a system in which a single predator adapts to a single prey. Second, we investigated the joint evolution of the body size and prey-size preference of a single predator confronted with a range of prey sizes. Third, we considered the adaptive radiation of predator types caused by resource competition. Fourth, we included trophic interactions among predators to examine their effects on the outcomes of predator radiation. Fifth, we included evolutionary stochasticity in our model, to corroborate the robustness of our deterministic predictions.

Figure 3 shows that when a single predator adapts to a single prey, predator body size is positively correlated with prey body size, with a slope equal to 1. This implies that the predators evolve to a fixed predator–prey size ratio that is constant across predator sizes. A positive correlation between body sizes of predator and prey is indeed found in vertebrates (Gittleman 1985; Vezina 1985) and invertebrates (Warren and Lawton 1987), as well as in planktonic predators (Hansen et al. 1994). Even though these studies underscore that a general and fixed size ratio does not exist, they do find a constant size ratio within each trophic or taxonomic group.

When, instead of one prey size, a range of prey sizes is available simultaneously to the predator, and the body size and prey-size preference of a single predator evolve jointly, the size ratio at the resultant evolutionary equilibrium (asterisk in Fig. 3) is slightly different from that resulting from single-trait evolution (dashed line in Fig. 3). This is because now a range of prey sizes is available, so that the predator's niche width comes to play a role. The effects of varying this niche width are discussed in detail in Section "Evolutionary effects of feeding modes".

Were the range of prey sizes not bounded, the predators would evolve towards ever smaller body sizes. This is inherent to their physiology, which favors small sizes over large ones: large organisms have relatively more energy reserves, and therefore a relatively longer egg-production period, which negatively affects their reproduction rate. Also, smaller organisms have a relatively large surface area, which is favorable with respect to the encounter and ingestion rates which both scale with surface area. Apparently, many physiological mechanisms favor a smaller size. Two factors that, by contrast, may induce evolution towards larger body sizes are heat loss and environmental variability. The tendency of organisms living at high latitudes to evolve to large body sizes has become known as Bergmann's rule (Bergmann 1847; Mayr 1956, 1963), and is often ascribed to the favorable effects of lower surface-area-to-volume ratios on heat loss. Environmental variability brings about periods of elevated starvation danger against which a large body size protects, as larger organisms possess larger energy reserves. These two factors, however, were not considered in the present study.

Figure 3 (filled circles) shows the trait combinations of the predator populations that will eventually result from deterministic evolution when adaptive radiations are

considered. The mechanism underlying the evolutionary branching events is competition for resources, which leads to disruptive selection. The evolutionary branching process affects both adaptive traits: under the force of disruptive selection, some populations evolve towards smaller body sizes and smaller prey-size preferences, while others evolve to larger body sizes and larger prey-size preferences. When they are isolated, each of the populations (filled circles) will again evolve towards the first evolutionary equilibrium (asterisk). The latter may correspond to evolutionary processes on some islands, where small mammal species have been observed to evolve to a larger size and larger species to a smaller size. Such a tendency has become known as the 'island rule' (Van Valen 1973), and can thus be understood by the evolutionary dynamics in our model. Figure 3 also shows that all resulting populations retain the same predator–prey size ratio. From this it can be concluded that competition for resources may lead to the differentiation of predator body sizes and prey-size preferences, but not to a differentiation of predator–prey size ratios.

In determining these evolutionary outcomes, direct interactions among predators, either through predation or through interference competition, were not taken into account. Therefore, these outcomes clearly correspond to idealized conditions. Real organisms may only conform to the resultant predictions in situations in which competition and predation among predators are naturally absent.

Predation among predators or direct (interference) competition, on the other hand, may give an additional advantage to large body sizes:larger organisms can be preyed upon by a smaller range of predators and are thus less vulnerable to predation (as follows from the triangular distribution of empirical predator–prey combinations), and they may also have an advantage in the direct competition for food or territory. As such, these processes may be expected to cause organisms to depart from the predator–prey size ratios predicted above.

Figure 3 (open circles) shows that predation among predators does indeed lead to much larger predator–prey size ratios than would be expected on the basis of resource competition alone. Predation among predators may thus indeed be an important factor for explaining the large variation of predator–prey size ratios found in nature. Direct (interference) competition is expected to have a similar effect as predation among predators. Both factors help explain Cope's rule (Cope 1896; Benton 2002), which states that natural selection will tend to produce large-bodied species.

Predictions of deterministic and stochastic renderings of the evolutionary dynamics in our model agree almost completely, even though the stochastic dynamics expectedly induce a slight amount of jitter in the evolved predator communities (open circles in Fig. 3).

Evolutionary effects of environmental factors

Figures 4a and b show how the outcomes of evolution in predator body size and prey-size preference are affected by the availability of prey sizes. An increase in the mean $\tilde{\mu}$ of the prey-size distribution causes both traits to increase (Fig. 4a), while the response to variations in the standard deviation σ of the prey-size distribution turns out to be hump-shaped (Fig. 4b). Although the evolved values of the scaled predator body size $\tilde{\ell}_{\mathrm{A}}$ and prey-size preference $\tilde{\ell}_{\mathrm{P}}$ change, their ratio remains essentially constant across a large range of the studied parameter values. Changes in the prey-size distribution, expressed in terms of $\tilde{\mu}$

and σ, may thus induce shifts in predator body sizes and prey-size preferences, but cannot explain the variation observed in predator–prey size ratios.

In contrast, an increase in dilution rate does change the evolved size ratio by making it larger. The evolved body size of predators is affected by the dilution rate through changes in food abundance: smaller dilution rates reduce both the rate at which new prey enter the system and the mortality of predators, thus intensifying conspecific competition for resources. The resulting decrease in evolved predator body size may correspond to the tendency to dwarfism on islands, which also has been related to limited food resources (Case 1978).

Evolutionary effects of feeding modes

Ecological factors, such as the predator's feeding mode, may also affect the evolutionary outcomes of predator body size and prey-size preference. In particular, a difference between the predator–prey size ratio of filter feeders and raptorial feeders is seen across taxonomic groups. Hansen et al. (1994) found that the optimal size ratio of filter feeders is larger than that of raptorial feeders. They also found that filter feeders generally feed on a larger range of prey sizes than raptorial feeders. To examine whether the wider prey range can explain the differences in size ratios, we studied the evolutionary effects of varying the niche width σ_P of the predator. Figure 5a shows that the predator–prey size ratio first increases with niche width and then stabilizes. As the niche width goes to zero, the predator evolves towards a preference for the smallest prey size that is still available. In this case, the predator–prey size ratio becomes equal to the size ratio that was predicted from single-trait evolution; this is expected, as in that analysis the predator was assumed to feed on one prey size only, which corresponds to vanishing niche width.

Although raptorial feeders may be more size-selective, it is conceivable that they are also more efficient predators, with a larger fraction of their attacks being successful. Therefore, we also studied the evolutionary effects of varying the capture efficiency ρ_s. Figure 5b shows that when a predator is less successful, its body size will become larger, while its prey-size preference will become smaller. Successful predators will thus evolve towards smaller predator–prey size ratios. Combining a large niche width with a small capture efficiency will lead to an even stronger increase in predator–prey size ratio, which may explain the large size ratio often encountered in filter feeders. These mechanisms might also provide an explanation for the tendency of the predator–prey size ratio to decrease with trophic level (Cohen et al. 2003), as predators at higher trophic levels may more often be raptorial feeders than filter feeders.

Conclusions

A size-dependent functional response was developed and combined with body-size scaling relationships from DEB theory to establish a physiologically motivated eco-evolutionary model of adaptations in the body sizes and prey-size preferences of predators. To obtain a realistic coexistence set for feasible predator–prey size combinations, we included capture times that depend on predator–prey size ratios. The resulting model exhibits many features, both ecological and evolutionary, that match empirical observations, such as the triangular distribution of predator–prey size combinations, the island rule, dwarfing, and the difference in predator–prey size ratio between filter feeders and raptorial feeders.

The coexistence set predicted by our model accommodates a wide range of predator–prey size ratios. By contrast, the evolutionary outcomes in the simplest versions of our model, in which a single predator adapts either to a single prey or to a range of prey, imply a fixed predator–prey size ratio. Even though such a fixed size ratio often exists within trophic and taxonomic groups, it certainly does not apply across these groups. We therefore introduced and examined various factors that may help explain variation in predator–prey size ratios. These factors can be organized into three different classes (Fig. 6).

First, some factors may change the size ratio predicted for single-predator adaptation (Fig. 6a). Therefore, these factors can have a large impact on observed patterns of predator–prey size combinations. Examples include changes in physiology and feeding mode, but also changes in food abundance. Within taxonomic or trophic groups, organisms often possess a relatively similar physiology, which may therefore explain the constant size-ratio that is observed within such groups. It should be noted that factors in this class, in contrast to those listed further below, may also affect the boundaries of the coexistence set. Yet, on the logarithmic scale used in Figs. 1–3, the resultant lower boundaries of the coexistence set lie close to each other for a relatively large range of parameter values.

Second, there are other factors that cause predators to change their body size and prey-size preference without changing their predator–prey size ratio (Fig. 6b). These include, for example, changes in the range of available prey sizes. Also, the patterns of size combinations resulting from resource competition conform to a fixed predator–prey size ratio. In addition, our analysis has demonstrated that competition for resources induces differentiation, rather than mere shifts, in predator body sizes and prey-size preferences. Changes in the available range of prey sizes and resource competition may thus explain the range of predator body sizes and prey-size preferences observed in nature, but cannot explain the large variation in predator–prey size ratios.

Third, some factors may systematically induce organisms to depart from the predator–prey size ratio predicted for single-prey-single-predator adaptation (Fig. 6c). We have found that predation among predators, as well as interference competition, can cause this effect, by giving an additional advantage to large body sizes. As such, these processes may

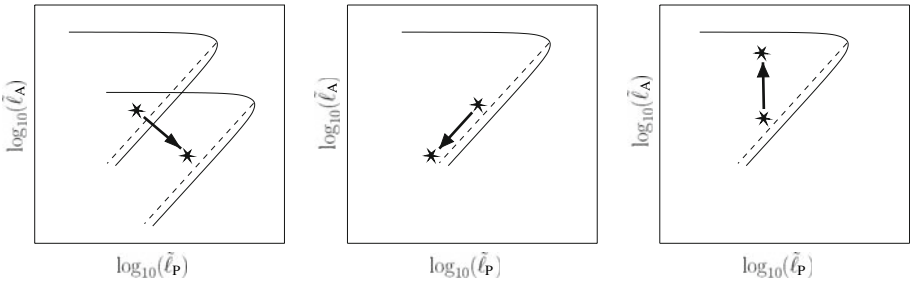

Fig. 6 Three different types of change in evolved predator–prey patterns. Continuous curves delineate the boundaries of the coexistence set, dashed lines show the outcomes of single-trait evolution, and asterisks indicate the evolutionary outcome of two-trait predator evolution when a range of prey types is present. Arrows depict changes in the predator's two adaptive traits $\tilde{\ell}_A$ (vertical) and prey-size preference $\tilde{\ell}_P$ (horizontal): (**a**) the expected outcome of evolution in predator body size and predator–prey size ratio is changed, together with the coexistence set; (**b**) predator body size evolves, while the predator–prey size ratio remains the same; (**c**) the predator evolves away from the body size and size ratio predicted by single-trait predator evolution

provide an explanation for the tendency of natural selection to produce large-bodied species (Cope's rule). Factors from this third class also help us understand the diversity of predator–prey size ratios encountered in nature.

Distinguishing which of these types of processes is causing the variation in specific empirical predator–prey size combinations will not be easy. Several parameters and processes have similar, or compensatory, effects that are difficult to separate, even in experiments. For example, in most cases it will be problematic to assess the evolutionary outcome of single-prey-single-predator adaptation. This is because the organism will usually have adapted evolutionarily to its specific environment, which typically includes predation and competition. These limitations should be taken into account when trying to explain empirical predator–prey patterns, or when measuring predator–prey size ratios in experimental setups.

Acknowledgments T. A. Troost thanks the International Institute for Applied Systems Analysis (IIASA) in Austria for providing the possibility of a three-month stay during which the basis for this paper was laid out, and the Netherlands Organization for Scientific Research (NWO) for financing this stay. The authors are very grateful for the data kindly provided by J. Cohen, S. Pimm, P. Yodzis, and J. Saldaña, previously published in Cohen et al. (1993), and for their approval to use them in Fig. 2. We also would like to thank M. Boer, O. Diekmann, F. Kelpin, and M. Kirkilionis for helpful discussions on DDEs. Furthermore, we would like to thank two anonymous referees for their comments which have considerably improved the paper. U. Dieckmann gratefully acknowledges financial support by the European Marie Curie Research Training Network FishACE (Fisheries-induced Adaptive Changes in Exploited Stocks), funded by the European Communitys Sixth Framework Programme.

Appendix: Derivation of invasion fitness

In this appendix we show that for determining the invasion fitness of the DDE system Eq. 12 one can use an ODE formulation without delay. For this purpose, below we derive the invasion fitness of a mutant predator trying to invade a given resident population of predators. For determining the coexistence set a formulation without delay can be derived as well, which we will not demonstrate explicitly, since that derivation is very similar to the one presented below.

We start from the DDE system Eq. 12, consisting of a prey population x_1 and a resident predator population $x_{\mathrm{A,r}}$, and introduce a mutant predator population $x_{\mathrm{A,m}}$ according to Eq. 14. For the sake of clarity, we consider only a single prey population and leave out the tildes that denote scaled parameters in the main text. The derivation of the invasion fitness for multiple prey requires just a few adjustments, as is explained at the end of this appendix. The resulting full system is given by

$$\frac{\mathrm{d}x_1(\tau)}{\mathrm{d}\tau} = \big(x_{r,1} - x_1(\tau)\big)D - I_{1,\mathrm{r}}f_{1,\mathrm{r}}(\tau)x_{\mathrm{A,r}}(\tau) - I_{1,\mathrm{m}}f_{1,\mathrm{m}}(\tau)x_{\mathrm{A,m}}(\tau), \tag{21a}$$

$$\frac{\mathrm{d}x_{\mathrm{A,r}}(\tau)}{\mathrm{d}\tau} = R_{\mathrm{r}}(\tau - a_{\mathrm{b,r}})\exp(-h_{\mathrm{r}}a_{\mathrm{b,r}})x_{\mathrm{A,r}}(\tau - a_{\mathrm{b,r}}) - h_{\mathrm{r}}x_{\mathrm{A,r}}(\tau), \tag{21b}$$

$$\frac{\mathrm{d}x_{\mathrm{A,m}}(\tau)}{\mathrm{d}\tau} = R_{\mathrm{m}}(\tau - a_{\mathrm{b,m}})\exp(-h_{\mathrm{m}}a_{\mathrm{b,m}})x_{\mathrm{A,m}}(\tau - a_{\mathrm{b,m}}) - h_{\mathrm{m}}x_{\mathrm{A,m}}(\tau). \tag{21c}$$

We assume that there is a stable equilibrium of the prey-resident system, Eq. 21 for $x_{\mathrm{A,m}}(\tau) = 0$, at which the resident predator population has positive density. We confirmed this assumption numerically for the coexistence set shown in Fig. 1 using the default parameter values given in Table 2.

The subsequent analysis can be outlined as follows. In order to derive the mutant's invasion fitness, we study the stability of the full system after the mutant has been introduced at the prey-resident equilibrium. The full prey-resident-mutant system above is then linearized around this equilibrium, and the characteristic equation of the resultant linear system is analyzed. When the real parts of all roots of this equation are negative, the resident is stable and the mutant cannot invade. By contrast, when the dominant root is positive, the resident is unstable and the mutant can invade. In particular, we will determine the combinations of trait values at which this stability changes.

Below, a superscripted asterisk indicates that the considered variable is at equilibrium under constant environmental conditions. We now introduce new variables that denote displacements from this equilibrium,

$$\begin{aligned} \xi_1 &= x_1 - x_1^*, \\ \xi_{\mathrm{A,r}} &= x_{\mathrm{A,r}} - x_{\mathrm{A,r}}^*, \\ \xi_{\mathrm{A,m}} &= x_{\mathrm{A,m}} - x_{\mathrm{A,m}}^*. \end{aligned} \tag{22}$$

The linearized model at equilibrium then reads

$$\begin{aligned} \frac{\mathrm{d}\xi_1(\tau)}{\mathrm{d}\tau} = &-\xi_1(\tau)D - I_{1,\mathrm{r}}\left(\xi_1(\tau)\frac{\mathrm{d}f_{1,\mathrm{r}}}{\mathrm{d}x_1}(x_1^*)x_{\mathrm{A,r}}^* + f_{1,\mathrm{r}}(x_1^*)\xi_{\mathrm{A,r}}(\tau)\right) \\ &- I_{1,\mathrm{m}}\left(\xi_1(\tau)\frac{\mathrm{d}f_{1,\mathrm{m}}}{\mathrm{d}x_1}(x_1^*)x_{\mathrm{A,m}}^* + f_{1,\mathrm{m}}(x_1^*)\xi_{\mathrm{A,m}}(\tau)\right), \end{aligned} \tag{23a}$$

$$\frac{\mathrm{d}\xi_{\mathrm{A,r}}(\tau)}{\mathrm{d}\tau} = \left(\xi_1(\tau - a_{\mathrm{b,r}})\frac{\mathrm{d}R_{\mathrm{r}}}{\mathrm{d}x_1}(x_1^*)x_{\mathrm{A,r}}^* + R_{\mathrm{r}}(x_1^*)\xi_{\mathrm{A,r}}(\tau - a_{\mathrm{b,r}})\right)\exp(-h_{\mathrm{r}}a_{\mathrm{b,r}}) - h_{\mathrm{r}}\xi_{\mathrm{A,r}}(\tau), \tag{23b}$$

$$\begin{aligned} \frac{\mathrm{d}\xi_{\mathrm{A,m}}(\tau)}{\mathrm{d}\tau} = &\left(\xi_1(\tau - a_{b\mathrm{m}})\frac{\mathrm{d}R_{\mathrm{m}}}{\mathrm{d}x_1}(x_1^*)x_{\mathrm{A,m}}^* + R_{\mathrm{m}}(x_1^*)\xi_{\mathrm{A,m}}(\tau - a_{\mathrm{b,m}})\right)\exp(-h_{\mathrm{m}}a_{\mathrm{b,m}}) \\ &- h_{\mathrm{m}}\xi_{\mathrm{A,m}}(\tau). \end{aligned} \tag{23c}$$

In the following we use the shorthand notations $R_{\mathrm{r}}^* = R_{\mathrm{r}}(x_1^*)$ and $R_{\mathrm{m}}^* = R_{\mathrm{m}}(x_1^*)$.

Since we are interested in the invasion by a rare mutant population, we take $x_{\mathrm{A,m}}^* = 0$. Then the matrix $\mathcal{P}$, defined by

$$\mathcal{P}\begin{pmatrix} \zeta_1 \\ \zeta_{\mathrm{A,r}} \\ \zeta_{\mathrm{A,m}} \end{pmatrix} = \begin{pmatrix} 0 \\ 0 \\ 0 \end{pmatrix}, \tag{24}$$

is obtained by substituting ξ_i in Eq. 23 by $\xi_i = \zeta_i \exp(\lambda\tau)$, $i = 1$, (A,r), (A,m) and division by $\exp(\lambda\tau) > 0$,

$$\mathcal{P} = \left(\begin{array}{ccc|c} & & & -I_{1,\mathrm{m}}f_{1,\mathrm{m}}(x_1^*) \\ & \mathcal{J}_1 & & \\ & & & 0 \\ \hline - & - & - & - \quad - \quad - \quad - \quad - \quad - \\ 0 & & 0 & \\ & & & \mathcal{J}_2 \end{array}\right) \tag{25}$$

The 2×2 matrix $\mathcal{J}_1$ is given by

$$\mathcal{J}_1 = \begin{pmatrix} -(\lambda + h_\mathrm{r}) - I_{1,\mathrm{r}} \frac{\mathrm{d}f_r}{\mathrm{d}x_1}(x_1^*)x_{\mathrm{A,r}}^* & -I_{1,\mathrm{r}} f_{1,\mathrm{r}}(x_1^*) \\ \exp(-(\lambda + h_\mathrm{r})a_{\mathrm{b,r}}) \frac{\mathrm{d}R_r}{\mathrm{d}x_1}(x_1^*)x_{\mathrm{A,r}}^* & R_\mathrm{r}^* \exp(-(\lambda + h_\mathrm{m})a_{\mathrm{b,r}}) - (\lambda + h_\mathrm{m}) \end{pmatrix} \tag{26}$$

and the 1×1 matrix $\mathcal{J}_2$ by

$$\mathcal{J}_2 = R_\mathrm{m}^* \exp(-(h_\mathrm{m} + \lambda)a_{\mathrm{b,m}}) - (\lambda + h_\mathrm{m}). \tag{27}$$

The characteristic equation is obtained by the requirement that the determinant of the matrix $\mathcal{P}$ be equal to zero. Then the ζ_i play the role of eigenvector components and the complex number λ plays the role of eigenvalue, which is now a root of the characteristic equation.

Since the mutant is assumed to be rare, the determinant of $\mathcal{P}$ factorizes, being given by the product of $\det\mathcal{J}_1$ and $\det\mathcal{J}_2 = \mathcal{J}_2$, with these two factors corresponding to the two decoupled systems: the prey-resident system without the mutant (i.e., $x_{\mathrm{A,m}}^* = 0$), described by $\mathcal{J}_1$, and the growth rate of the mutant population, described by $\mathcal{J}_2$.

The first factor yields the characteristic equation of the prey-resident system, $\det\mathcal{J}_1 = 0$. This characteristic equation belongs to the eigenvalue problem for the set of one ODE and one DDE given by Eq. 23a, without the last term, and Eq. 23b, evaluated at the equilibrium of the prey-resident system.

The second factor yields the characteristic equation $\det\mathcal{J}_2 = \mathcal{J}_2 = 0$ of the first-order linear homogeneous DDE (Eq. 23c) describing the specific growth rate of the mutant population. The expression for $\mathcal{J}_2$ in Eq. 27 is of a form discussed extensively by Diekmann et al. (1995, p. 312). For this case, the complex roots of the characteristic equation can be obtained analytically.

The function $\mathcal{J}_2(\lambda)$ with $\lambda \in \mathbf{R}$ is monotonically decreasing, $d\mathcal{J}_2/d\lambda < 0$. Therefore there is one unique real root λ_0. Since $\mathcal{J}_2(0) = R_\mathrm{m}^* \exp(-h_\mathrm{m}a_{\mathrm{b,m}}) - h_\mathrm{m}$, the real eigenvalue equals zero, $\lambda_0 = 0$, if and only if $R_\mathrm{m}^*\exp(-h_\mathrm{m}a_{\mathrm{b,m}}) = h_\mathrm{m}$. Thus, Eq. 27 has exactly one positive real solution, $\lambda_0 > 0$, when $R_\mathrm{m}^*\exp(-h_\mathrm{m}a_{\mathrm{b,m}}) > h_\mathrm{m}$ and exactly one negative real solution, $\lambda_0 < 0$, when $R_\mathrm{m}^*\exp(-h_\mathrm{m}a_{\mathrm{b,m}}) < h_\mathrm{m}$. Further, (Driver 1977, p. 321) showed that equations of this form have infinitely many complex roots. Let $\lambda_k = \mu_k + i\omega_k$; then substitution of this into the characteristic equation $\mathcal{J}_2 = 0$ and separately equating real and imaginary parts gives

$$\mu_k = \exp(-\mu_k a_{\mathrm{b,m}})R_\mathrm{m}^* \exp(-h_\mathrm{m}a_{\mathrm{b,m}}) \cos(a_{\mathrm{b,m}}\omega_k) - h_\mathrm{m}, \tag{28}$$

$$\omega_k = -\exp(-\mu_k a_{\mathrm{b,m}})R_\mathrm{m}^* \exp(-h_\mathrm{m}a_{\mathrm{b,m}}) \sin(a_{\mathrm{b,m}}\omega_k). \tag{29}$$

Clearly, if Eq. 29 holds for ω_k, it holds also for $-\omega_k$, so the complex conjugate $\lambda_k^* = \mu_k - i\omega_k$ is also a root of the characteristic equation. Furthermore, the unique real root λ_0 is the dominant eigenvalue, i.e., the real parts of all other roots are smaller than λ_0. This can be seen as follows. Comparison of Eq. 28 with the characteristic equation for λ_0 gives

$$\lambda_0 - \mu_k = \big(1 - \exp((\lambda_0 - \mu_k)a_{\mathrm{b,m}}) \cos(a_{\mathrm{b,m}}, \omega_k)\big)R_\mathrm{m}^* \exp(-h_\mathrm{m}a_{\mathrm{b,m}}). \tag{30}$$

Suppose that $\cos(a_{\mathrm{b,m}}\omega_k) = 1$, then $\sin(a_{\mathrm{b,m}}\omega_k) = 0$, and hence $\omega_k = 0$, which contradicts the fact that $\lambda_k = \mu_k + i\omega_k$ has non-zero imaginary part. We can thus conclude that $\cos(a_{\mathrm{b,m}}\omega_k) < 1$. Now assume that $\lambda_0 - \mu_k \leq 0$, then, with $R_\mathrm{m}^* > 0$ (since $R_\mathrm{m}^* \approx R_\mathrm{r}^* > 0$ due to small mutational steps), Eq. 30 implies $1 \leq \exp((\lambda_0 - \mu_k)\, a_{\mathrm{b,m}}) \cos(a_{\mathrm{b,m}}\omega_k)$, and also this

leads to a contradiction. This shows that Re $(\lambda_k) < \lambda_0$, $k = 1, 2, \ldots$, or in other words: the real eigenvalue λ_0 is the dominant root of the characteristic equation $\det \mathcal{J}_2 = 0$.

We had mentioned above that the prey-resident system has a positive stable equilibrium for the default parameter values given in Table 2. Under these circumstances, the real parts of the eigenvalues of $\mathcal{J}_1$ are strictly negative. Thus, the dominant eigenvalue λ_0 of $\mathcal{J}_2$ will also be the dominant eigenvalue of $\mathcal{P}$, if this λ_0 exceeds the largest real part of the eigenvalues of $\mathcal{J}_1$. Hence, for $\det \mathcal{J}_2 = 0$, that is, for $R^*_{\mathrm{m}} \exp(-h_{\mathrm{m}} a_{\mathrm{b,m}}) = h_{\mathrm{m}}$, the dominant eigenvalue of $\mathcal{P}$ will equal λ_0 and thus zero. At trait values for which this holds, the prey-resident-mutant system changes stability, so that the prey-resident system becomes invadable by the mutant predator.

Now suppose that the real eigenvalue λ_0 is positive but small. Then the characteristic equation of $\mathcal{J}_2$ gives

$$\begin{aligned}\lambda_0 &= R^*_{\mathrm{m}} \exp(-(\lambda_0 + h_{\mathrm{m}}) a_{\mathrm{b,m}}) - h_{\mathrm{m}} \\ &= \left(1 - \lambda_0 a_{\mathrm{b,m}} + \frac{1}{2}\lambda_0^2 a_{\mathrm{b,m}}^2 + \cdots\right) R^*_{\mathrm{m}} \exp(-h_{\mathrm{m}} a_{\mathrm{b,m}}) - h_{\mathrm{m}},\end{aligned}$$

so that, for $\lambda_0 a_{\mathrm{b,m}} \ll 1$, we have

$$\lambda_0 = R^*_{\mathrm{m}} \exp(-h_{\mathrm{m}} a_{\mathrm{b,m}}) - h_{\mathrm{m}}. \tag{31}$$

Consequently, the rate λ_0 is the invasion fitness of the mutant predator at the equilibrium of the prey-resident system, ($x^*_1 > 0$, $x^*_{\mathrm{A,r}} > 0$, $x^*_{\mathrm{A,m}} = 0$).

We have thus shown that, if $\lambda_0 a_{\mathrm{b,m}} \ll 1$, which holds for small mutational steps, the invasion fitness can be determined by a formulation without delay, corroborating our approach in the main text (Eq. 15). The rare mutant ($x_{\mathrm{A,m}} \to 0$) will be able to invade the stable prey-resident system if and only if $R^*_{\mathrm{m}} \exp(-h_{\mathrm{m}} a_{\mathrm{b,m}}) > h_{\mathrm{m}}$. The biological interpretation of this inequality is clear: the mutant's effective birth rate has to exceed the dilution rate. After successful invasion, the mutant generally replaces the resident (Geritz et al. 2002); around evolutionary branching points they can coexist, leading to a dimorphic predator population (Metz et al. 1992, 1996; Geritz et al. 1997, 1998).

For the (ecological) stability at the boundaries of the coexistence set a formulation without delay can be derived as well. This derivation is very similar to that of the invasion fitness explained above, but simpler, as no mutants are considered but only the prey and resident predator populations. The resulting condition fulfilled at the boundaries of the coexistence set is given by $R^* \exp(-h a_{\mathrm{b}}) = h$.

Considering multiple prey populations instead of a single one will affect system Eq. 21 in two ways. First, the dynamics of each prey population are described by a separate equation, such that for n prey populations, the full system will consist of $n + 2$ equations. Second, the prey populations will affect the growth rate R (Eq. 13) of the predators (both residents and mutants) through their functional response f (Eq. 6). The derivation of the invasion fitness itself, however, is largely analogous to that shown above. The determinant of the matrix $\mathcal{P}$ is still factorizable, and remains given by the product of $\det \mathcal{J}_1$ and $\det \mathcal{J}_2$. $\mathcal{J}_2$ is still given by Eq. 27, adjusted for multiple prey through f in R. $\mathcal{J}_1$ will now be a $(n + 1) \times (n + 1)$ matrix, which corresponds to the system of the resident predator and the n prey populations without the mutant predator. Supported by the simulation results, we again assume that the system without the mutant is stable. It is then easy to see that the invasion fitness for multiple prey resembles that for a single prey (Eq. 31), adjusted through f in R.

References

Aljetlawi AA, Sparrevik E, Leonardsson K (2004) Prey-predator size-dependent functional response: derivation and rescaling to the real world. J Anim Ecol 73(2):239–252

Alver MO, Alfredsen JA, Olsen Y (2006) An individual-based population model for rotifer (*Brachionus plicatilis*) cultures. Hydrobiologia 560:93–208

Benton MJ (2002) Cope's rule. In: Pagel M (ed) Encyclopedia of evolution. Oxford University Press, Oxford, pp 185–186

Bergmann C (1847) Über die Verhältnisse der Wärmeökonomie der Thiere zu ihre Grösse. Gött Stud 3: 595–708

Brown JH, Marquet PA, Taper ML (1993) Evolution of body size: consequences of an energetic definition of fitness. Am Nat 142(4):573–584

Case TJ (1978) Endothermy, and parental care in the terrestrial vertebrates. Am Nat 112(987):861–874

Cohen JE (1989) Food webs and community structure. In: Roughgarden J, May RM, Levin SA (eds) Perspectives on ecological theory. Princeton University Press, Princeton, pp 181–202

Cohen JE, Jonsson T, Carpenter SR (2003) Ecological community description using the food web, species abundance, and body size. Proc Natl Acad Sci USA 100(4):1781–1786

Cohen JE, Newman CM (1985) A stochastic theory of community food webs 1. Models and aggregated data. Proc R Soc Lond B, Biol Sci 224(1237):448–461

Cohen JE, Pimm SL, Yodzis P, Saldana J (1993) Body sizes of animal predators and animal prey in food webs. J Anim Ecol 62(1):67–78

Combes C (2001) Parasitism; the ecology and evolution of intimate interactions. University of Chicago Press

Cope ED (1896) The primary factors of organic evolution. The Open Court Publishing Company, Chicago

Dieckmann U (1997) Can adaptive dynamics invade? Trends Ecol Evol 12(4):128–131

Dieckmann U, Law R (1996) The dynamical theory of coevolution: a derivation from stochastic processes. J Math Biol 34(5–6):579–612

Diekmann O, van Gils SA, Verduyn Lunel SM, Walther H-O (1995) Delay equations: functional-, complex- and nonlinear analysis, Volume 110 of Applied Mathematical Sciences. Springer-Verlag, New York

Driver RD (1977) Ordinary and delay differential equations, Volume 20 of Applied Mathematical Sciences. Springer-Verlag, New York

Ellis T, Gibson RN (1997) Predation of 0-group flatfishes by 0-group cod: handling times and size-selection. Mar Ecol Prog Ser 149(1–3):83–90

Forsman A (1996) Body size and net energy gain in gape-limited predators: a model. J Herpetol 30(3): 307–319

Geritz SAH, Gyllenberg M, Jacobs FJA, Parvinen K (2002) Invasion dynamics and attractor inheritance. J Math Biol 44(6):548–560

Geritz SAH, Kisdi É, Meszéna G, Metz JAJ (1998) Evolutionarily singular strategies and the adaptive growth and branching of the evolutionary tree. Evol Ecol 12(1):35–57

Geritz SAH, Metz JAJ, Kisdi É, Meszéna G (1997) Dynamics of adaptation and evolutionary branching. Phys Rev Lett 78(10):2024–2027

Gittleman JL (1985) Carnivore body size: ecological and taxonomic correlates. Oecologia 67(4):540–554

Hansen B, Bjornsen PK, Hansen PJ (1994) The size ratio between planktonic predators and their prey. Limnol Oceanogr 39(2):395–403

Husseman JS, Murray DL, Power G, Mack C, Wenger CR, Quigley H (2003) Assessing differential prey selection patterns between two sympatric large carnivores. Oikos 101(3):591–601

Karpouzi V, Stergiou KI (2003) The relationships between mouth size and shape and body length for 18 species of marine fishes and their trophic implications. J Fish Biol 62(6):1353–1365

Kooi BW, Kooijman SALM (1997) Population dynamics of rotifers in chemostats. Nonlinear Anal Theory Meth Appl 30(3):1687–1698

Kooi BW, Kooijman SALM (1999) Discrete event versus continuous approach to reproduction in structured population dynamics. Theor Popul Biol 56(1):91–105

Kooijman SALM (1986) Energy budgets can explain body size relations. J Theor Biol 121:269–282

Kooijman SALM (2000) Dynamic energy and mass budgets in biological systems. Cambridge University Press

Kooijman SALM (2001) Quantitative aspects of metabolic organization; a discussion of concepts. Philos Trans R Soc B, Biol Sci 356(1407):331–349

Kristiansen JN, Fox T, Nachman G (2000) Does size matter? Maximising nutrient and biomass intake by shoot size selection amongst herbivorous geese. Ardea 88(2):119–125

Loeuille N, Loreau M (2005) Evolutionary emergence of size-structured food webs. Proc Natl Acad Sci USA 102(16):5761–5766
Manatunge J, Asaeda T (1998) Optimal foraging as the criteria of prey selection by two centrarchid fishes. Hydrobiologica 391(1–3):223–240
Mayr E (1956) Geographical character gradients and climatic adaptation. Evolution 10(1):105–108
Mayr E (1963) Animal species and evolution. Harvard University Press, Cambridge, Mass
Mehner T, Plewa M, Hulsmann S, Worischka S (1998) Gape-size dependent feeding of age-0 perch (*Perca fluviatilis*) and age-0 zander (*Stizostedion lucioperca*) on daphnia galeata. Arch Hydrobiol 142(2): 191–207
Memmott J, Martinez ND, Cohen JE (2000) Predators, parasitoids and pathogens: species richness, trophic generality and body sizes in a natural food web. J Anim Ecol 69(1):1–15
Metz JAJ, Nisbet RM, Geritz SAH (1992) How should we define 'fitness' for general ecological scenarios? Trends Ecol Evol 7(6):198–202
Metz JAJ, Geritz SAH, Meszéna G, Jacobs FJA, van Heerwaarden JS (1996) Adaptive dynamics: A geometrical study of the consequences of nearly faithful reproduction. In: van Strien SJ, Verduyn Lunel SM (eds) Stochastic and spatial structures of dynamical systems. KNAW Verhandelingen, Amsterdam, pp 183–231
Neubert MG, Blumenshine SC, Duplisea DE, Jonsson T, Rashleigh B (2000) Body size and food web structure: testing the equiprobability assumption of the cascade model. Oecologia 123(2):241–251
Peters RH (1983) The ecological implications of body size. Cambridge University Press, New York
Rincon PA, Loboncervia J (1995) Use of an encounter model to predict size-selective predation by a stream-dwelling cyprinid. Freshw Biol 33(2):181–191
Rytkonen S, Kuokkanen P, Hukkanen M, Huhtala K (1998). Prey selection by sparrowhawks *Accipiter nisus* and characteristics of vulnerable prey. Ornis Fenn 75(2):77–87
Svensson JE (1997) Fish predation on *Eudiaptomus gracilis* in relation to clutch size, body size, and sex: A field experiment. Hydrobiologica 344(1–3):155–161
Turesson H, Persson A, Bronmark C (2002) Prey size selection in piscivorous pikeperch (*Stizostedion lucioperca*) includes active prey choice. Ecol Freshwa Fish 11(4):223–233
Van Valen L (1973). Pattern and the balance of nature. Evol Theory 1:31–49
Vezina AF (1985) Empirical relationships between predator and prey size among terrestrial vertebrate predators. Oecologia 67(4):555–565
Warren PH, Lawton JH (1987) Invertebrate predator-prey body size relationships: an explanation for upper triangular food webs and patterns in food web structure?. Oecologia 74(2):231–235
Williams RJ, Martinez ND (2000) Simple rules yield complex food webs. Nature 404(6774):180–183
Yodzis P, Innes S (1992) Body size and consumer-resource dynamics. Am Nat 139(6):1151–1175